Neurobiology of Disease 175 (2022) 105919

Contents lists available at ScienceDirect

Neurobiology of Disease

journal homepage: www.elsevier.com/locate/ynbdi

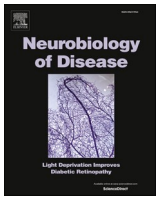

Cathepsin D: Analysis of its potential role as an amyloid beta degrading protease

Lisa Gallwitz [a], Lina Schmidt [a], André R.A. Marques [b], Andreas Tholey [c], Liam Cassidy [c], Irem Ulku [d], Gerhard Multhaup [d], Alessandro Di Spiezio [a,1], Paul Saftig [a,*,1]

[a] Institute of Biochemistry, Christian-Albrechts-University Kiel, 24118 Kiel, Germany
[b] iNOVA4Health, NOVA Medical School, Universidade NOVA de Lisboa, 1150-082 Lisbon, Portugal
[c] Systematic Proteomics and Bioanalytics – Institute for Experimental Medicine, Christian-Albrechts-University Kiel, 24105 Kiel, Germany
[d] Department of Pharmacology and Therapeutics, Faculty of Medicine and Health Sciences McGill University, Montreal, Canada

ARTICLE INFO

Keywords:
Cathepsin-D
Lysosome
Neuronal ceroid lipofuscinosis 10
Proteolysis
Amyloid beta
Amyloid precursor protein
Alzheimer's disease

ABSTRACT

Proteolysis catalyzed by the major lysosomal aspartyl protease cathepsin-D (CTSD) appears to be of pivotal importance for proteostasis within the central nervous system and in neurodegeneration. Neuronal Ceroid Lipofuscinosis (NCL) type 10 is caused by a lack of CTSD leading to a defective autophagic flow and pathological accumulation of proteins. We previously demonstrated a therapeutic-relevant clearance of protein aggregates after dosing a NCL10 mouse model with recombinant human pro-cathepsin-D (proCTSD). Similar results could be achieved in cells and mice accumulating α-synuclein. Prompted by these positive effects and our *in vitro* findings showing that cathepsin-D can cleave the Alzheimer's Disease (AD)-causing amyloid beta peptides (Aβ), we envisaged that such a treatment with proCTSD could similarly be effective in clearance of potentially toxic Aβ species.

We demonstrated that CTSD is able to cleave human $A\beta^{1-42}$ by using liquid chromatography-mass spectrometry. Intracerebral dosing of proCTSD in a NCL10 (CTSD knockout) mouse model revealed uptake and processing of CTSD to its mature and active form. However, the re-addition of CTSD did not obviously affect intracellular APP processing or the generation of soluble APP and Aβ-species. ProCTSD treated HEK cells in comparison with untreated cells were found to contain comparable levels of soluble and membrane bound APP and Aβ-species. Also, the early intracranial application (P1 and P20) of proCTSD in the 5xFAD mouse model did not change Aβ pathology, plaque number and plaque composition and neuroinflammation, however we observed an increased level of $A\beta^{1-42}$ in the CSF.

Our data confirm proteolytic cleavage of human $A\beta^{1-42}$ by CTSD but exclude a prominent role of CTSD in APP processing and Aβ degradation in our *in vitro* and *in vivo* models.

1. Introduction

Lysosomes are of pivotal importance for macromolecule and protein degradation (Saftig and Klumperman, 2009). Endocytosis, phagocytosis or autophagy deliver the substrates to lysosomal proteases. Cathepsins are the major lysosomal proteases. After synthesis in the endoplasmic reticulum as inactive pro-forms they transit to lysosomes where they are proteolytically processed to mature fully active forms (Katunuma, 2010). Cathepsins have been implicated in a wide range of cellular functions including bulk protein degradation, antigen processing and presentation, proprotein processing, degradation of matrix constituents and initiation of apoptotic processes.

The aspartyl protease cathepsin-D (CTSD) is ubiquitously expressed and plays a pivotal role in the central nervous system. This is reflected by a loss of cathepsin-D in mice and men leading to a severe congenital neurodegenerative disease classified as Neuronal Ceroid Lipofuscinosis type 10 (NCL10). Undegraded protein aggregates in neurons lead to cell death associated with premature death in patients and in a NCL10 mouse model (Saftig et al., 1995; Koike et al., 2000; Steinfeld et al., 2006). In contrast, cathepsin-B or cathepsin-L deficiency in mice does

* Corresponding author at: Biochemical Institute, Christian-Albrechts-University Kiel, Olshausenstr. 40, D-24098 Kiel, Germany.
E-mail address: psaftig@biochem.uni-kiel.de (P. Saftig).
[1] Equal senior authorship.

https://doi.org/10.1016/j.nbd.2022.105919
Received 2 August 2022; Received in revised form 30 October 2022; Accepted 3 November 2022
Available online 5 November 2022

not lead to such severe phenotypic changes indicating a redundant function of some cathepsins. However, mouse models harbouring a combined loss of cathepsin-B and -L share a comparable drastic phenotype as found in cathepsin-D knockout mice (Felbor et al., 2002; Di Spiezio et al., 2021). The predominant role of cathepsin-D is already indicated by the observation that it can constitute as much as 10% of the soluble lysosomal protein in rat liver. Cathepsin-D's concentration inside liver was estimated to reach 0.7 mM (Dean and Barrett, 1976). In early studies based on the inhibitor pepstatin it was estimated that cathepsin-D contributes to about 10–50% of lysosomal protein degradation (Dean, 1975).

Interestingly, the application of pro-CTSD in a NCL10 preclinical mouse model could accelerate lysosomal protein degradation. It led to clearance of the pathologically relevant protein aggregates and reduced gliosis and neurodegeneration (Di Spiezio et al., 2021; Marques et al., 2020). This type of protease replacement strategy also increased the life span of these mice (Marques et al., 2020). This strategy was used to provide additional protease activity to foster the proteolytic capacity of lysosomes. In an independent study intraocular administration of CTSD effectively restored the disrupted autophagy-lysosomal pathway and reduced the retinal degeneration by promoting the survival of photoreceptors and rod bipolar cells (Liu et al., 2022). The beneficial effect of adding recombinant human CTSD to disease models was also illustrated by recent findings in α-synucleinopathy models where application of pro-CTSD to cells and mice with enhanced synuclein pathology increased α-synuclein degradation (Prieto Huarcaya et al., 2022).

CSTD has also been implicated in the pathogenesis of Alzheimer's Disease (AD). Late onset AD had been linked with a variation in the gene encoding for CSTD (Davidson et al., 2006) which is also associated with an increase of $A\beta^{1-42}$ and tau in cerebrospinal fluid (Papassotiropoulos et al., 2002; Riemenschneider et al., 2006). It is of note that early studies already identified a degrading activity of cathepsin-D towards tau (Kenessey et al., 1997) and Aβ (Hamazaki, 1996; McDermott and Gibson, 1996). In a more recent study, cathepsin-D turned out to be one of the principal intracellular Aβ-degrading proteases that can influence Aβ42/40 ratios *via* differential degradation of $A\beta^{1-42}$ *vs.* $A\beta^{1-40}$ (Suire et al., 2020). An upregulation of CTSD as a possible adaptive response in AD neocortex was also described (Chai et al., 2019). Recently, lysosome activity has also been linked to the intraneuronal build-up of Aβ which later leads to neuronal cell death and extracellular Aβ-deposits (Lee et al., 2022).

The major hypothesis tested here was that an initiation of lysosomal proteolysis by endoproteolysis through CTSD could contribute to increased overall lysosomal proteolysis and autophagic flux after application of proCTSD and endogenous processing of the pro-form into the active form in lysosomes. Cathepsin-D application should reduce both the intracellular and extracellular levels of the neurotoxic and aggregation prone amyloid peptides. Using cell-based assays and studies in a preclinical NCL mouse model and the 5xFAD mouse model we observed efficient uptake of proCTSD which raised intra-lysosomal activity and expression of the mature active form of the protease. In the different experimental systems, however, a significant impact of the therapeutic enzyme on APP processing, Aβ levels, plaque formation and neuroinflammation was not observed. This finding suggests that a CTSD-based enzyme therapy may be inappropriate to modulate the Aβ-caused pathology in AD.

2. Results

2.1. Recombinant human pro-cathepsin-D (rhproCTSD) is self-activated in vitro and cleaves amyloid beta 1–42

A recombinantly expressed form of human pro-cathepsin-D (rhproCTSD) dosed to mouse models of neuronal ceroid lipofuscinosis (Marques et al., 2020) and α-synucleinopathy (Prieto Huarcaya et al., 2022) revealed its therapeutic value to remove protein aggregates including α-synuclein. The expression and activity of CTSD in connection with lysosomal proteolysis have been linked to the pathogenesis of AD and the processing and removal of amyloid peptides (Di Domenico et al., 2016). We were first interested to investigate wheather our rhproCTSD could also cleave $A\beta^{1-42}$ *in vitro*. The pro-form of CTSD does not display a considerable proteolytic activity which makes it attractive as a drug for *in vivo* dosing where it remains inactive in the interstitial fluid but is activated after endocytic uptake in cells and delivery to lysosomes. For the use *in vitro*, we supported self-activation of rhproCTSD by incubating it for at least 30 min at a lysosome-like pH of 4.5. Under this condition the enzyme was fully active (Fig. 1A) and was detected as a mature 30 kDa CTSD form by immunoblot analysis (Fig. 1B). When such a pre-activated fraction of 2 μg rhproCTSD was co-incubated for 15, 30 and 60 min with 100 μM $A\beta^{1-42}$ peptides and analyzed by liquid chromatography-mass spectrometry (LC-MS) specific cleavage fragments were observed. While the educts in our experiment contained <2% of pre-cleaved peptides, according to the summed peptide spectral matches (Supplementary Fig. S1), a number of hydrolysis products were observed after 15 min (Fig. 1C, D, Supplementary Fig. S1). In particular, hydrolysis C-terminal to Phe19, leading to two peptides with masses of 2314.50 Da (average mass) and 2217.61 Da, representing the N- and the C-terminal cleavage product, respectively, could be detected and confirmed by MS/MS experiments (Supplementary Fig. S1). The C-terminal fragment was additionally proteolyzed C-terminal to Leu34 after 15 min. In addition, further processing products of the N-terminal (cleavage C-terminal to Leu17) and the C-terminal fragment (loss of the N-terminal Phe20) were observed. The later, two products were further increased in abundance at longer incubation times. In a control, the $A\beta^{1-42}$ peptide/ rhproCTSD was additionally incubated with pepstatin A, an aspartyl protease inhibitor. Here, no cleavage products could be observed; the increased fraction of the oxidized peptide (Met35) compared to the educt is common for Met-containing peptides at elevated incubation times. In summary, rhproCTSD is able to rapidly degrade the $A\beta^{1-42}$ peptide under the chosen acidic *in vitro* conditions.

2.2. Intracranial dosing of rhproCTSD in an NCL10 model did not affect the expression of mouse Aβ-species

Having provided an *in vitro* proof of principle that rhproCTSD is able to proteolytically process $A\beta^{1-42}$ we tested if also an *in vivo* application of the pro-enzyme has an impact on APP amyloid peptide metabolism. Using the previously mentioned model of NCL10 ($CTSD^{-/-}$ knockout (KO) mice) (Koike et al., 2000) we intracranially dosed 0.1 mg rhproCTSD at postnatal day 1 and 20 (Fig. 2A). Cathepsin-D was taken up by neurons (MAP-2-positive cells) and microglia (Iba 1-positive cells) as demonstrated by fluorescence microscopy (Fig. 2B) and detection of the mature active form of cathepsin-D by immunoblot analysis (Fig. 2C). The therapeutic effect of rhproCTSD became evident since treated mice did not lose weight caused by the disease progression, compared to PBS injected mice (Supplementary Fig. S2A). Biochemical analysis of the brain lysates revealed that cathepsin-D deficiency did not alter the expression levels of the full-length form of the murine amyloid precursor protein (APP) as well as the level of the C-terminal APP fragments C99 and C83, respectively (Fig. 2C, D). Dosing the CTSD KO mice with rhproCTSD did also not change levels of APP and APP-C99. There was a ~ 40% decrease of APP-C83 levels after treatment indicating that this fragment could be subject to lysosomal CTSD degradation (Fig. 2D(ii)). Importantly, the soluble APP fragments showed a tendency towards decreased levels of sAPPα and sAPPβ in homogenates of CTSD KO brains (Fig. E). However, treatment did only mildly but not significantly increase these levels (Fig. 2F). By immunoblot, endogenous Aβ could not be detected in the membrane bound and soluble fractions of the brain homogenates (Fig. 2C, E). ELISA and MSD measurements of soluble (diethylamine, DEA), insoluble (formic acid, FA) and RIPA (complete cell lysis) fractions of $A\beta^{1-40}$ and $A\beta^{1-42}$ did not reveal a clear trend towards an anti-amyloid effect of the rhproCTSD application (Fig. 2G,

Supplementary Fig. S2 B). In summary, after intracranial dosing of rhproCTSD in the CTSD KO mice the enzyme was endocytosed by neurons and microglia and matured to the active form. However, this treatment did not obviously affect the processing of APP or the generation of soluble APP and Aβ fragments.

2.3. RhproCTSD application to human APP overexpressing cells

Although the CTSD KO (NCL10) mouse model is suitable to follow up the therapeutic effect of rhproCTSD dosage (Marques et al., 2020) the levels of APP and Aβ are very low and despite of a neurodegenerative phenotype and lysosomal dysfunction these mice do not develop typical AD pathologies (Koike et al., 2000). To investigate whether cathepsin-D would alter APP and Aβ metabolism we used HEK293 cells expressing the human wildtype APP or the swedish mutant of APP (APPswe) (Mullan et al., 1992). These cells as well as wildtype HEK293 cells were incubated for 48 h with 20 μg/ml rhproCTSD with or without Pepstatin A (PepA) (Fig. 3A). Cathepsin-D was taken up and processed to the proteolytically active forms (Fig. 3B). HEK cell lysates (Fig. 3B) and supernatants (Fig. 3D) were analyzed by immunoblot to quantify APP fragments (Fig. 3C,E). No changes in cell lysates of flAPP, APP-C83 and APP-C99 were noted (Fig. 3C). Interestingly, pepstatin A inhibition caused statistically significant upregulated levels of $A\beta^{1-42}$ (Fig. 3C(vi)). In the supernatant of the cultured cells (where the rhproCTSD was not self-activated; Supplementary Fig. S3) no effect on the levels of soluble APP fragments sAPPα and sAPPβ (Fig. 3E(i) and (ii)), as well no obvious change in levels of amyloid fragments ($A\beta^{1-37}$, $A\beta^{1-40}$ and $A\beta^{1-42}$, Fig. 3E (iii)-(v)) was observed.

2.4. Analysis of rhproCTSD uptake and Aβ clearance in an Alzheimer mouse model

The cell-based data suggest that application of rhproCTSD did not influence APP-dependent proteolysis. However, to exclude that this is limited to a specific cellular system and experimental set up with the chosen incubation times we decided to study the effect of the intracranially dosed therapeutic enzyme in a well-established AD mouse model. We have chosen the 5xFAD mice that express human APP mutations (Swedish (K670N/M671L), Florida (I716V), and London (V717I)) and presenilin transgenes (M146L and L286V). These mice are well suited to study AD-related pathology such as amyloid plaque formation, gliosis and Aβ-accumulation starting in two-month-old mice (Oakley et al., 2006). We took profit from our experiences with the dosing study in the NCL10 model where the therapeutic enzyme was intracranially delivered at postnatal day P1 and P20 and could be detected in brain lysates for >31 days (Marques et al., 2020). We hypothesized that such an early delivery of rhproCTSD would interfere with the early production of Aβ and the processing of APP in the 5xFAD mouse model. To adapt the previously established protocol to the 5xFAD mice we first analyzed mice at 2 and 3 months of age for soluble APP fragments and Aβ. Immunoblot analysis revealed that two-month old brains contained considerable levels of hsAPPα and minute levels of Aβ. Aβ species were clearly detectable by immunoblot in three-month-old brain lysates (Supplementary Fig. S4 A). Subsequently, we intracerebrally dosed the 5xFAD mice at P1 and P20 with rhproCTSD. Mice were sacrificed and their brains were analyzed at one, two or three months of age (Supplementary Fig. S4 B). The dosed enzyme was readily detectable as the mature and active form of CTSD in brain lysates of one-month-old mice (Fig. 4A). Sets of one-month-old (Fig. 4 A,B), two-month-old (Supplementary Fig. S4 C,D) and three-month-old (Fig. 4C,D) wild-type and 5xFAD mice either injected with PBS or with rhproCTSD were biochemically analyzed for soluble proteins (DEA fraction), membrane-bound proteins (RIPA fraction) and insoluble proteins (formic acid fraction). At one month of age (Fig. 4A) the rhproCTSD-dosed 5xFAD brain samples showed no obvious changes in the levels of sAPPα, sAPPβ and soluble Aβ (Fig. 4B(i)-(iii)) compared to the PBS-dosed 5xFAD. Also, in the RIPA fractions the levels of full-length APP, APP-CTFs C99 and C83 as well as the intracellular levels of Aβ (Fig. 4B(iv)-(vi)) did not change after treatment. Whereas mature CTSD was present in the cell lysates, this did not cause a change in the number of lysosomes as indicated by an unchanged level of the lysosomal membrane protein LAMP-1 (Fig. 4B(vii)). At two months of age (Supplementary Fig. S4 C, D) the immunoblot analysis confirmed the data from the one-month old cohort of mice. Here we quantified the amounts of $A\beta^{1-40}$ and $A\beta^{1-42}$ in wild-type and 5xFAD DEA, RIPA and FA fractions by ELISA and observed a trend towards upregulated $A\beta^{1-40}$ and $A\beta^{1-42}$ levels of the 5xFAD mice treated with rhpro-CTSD in all of the investigated fractions (Supplementary Fig. S4 E). At three months of age (Fig. 4C,D) we observed a slight but statistically significant decrease of APP-CTF83 (Fig. 4D(iv)) and LAMP-1 (Fig. 4D(vii)) after dosing. However, all other APP fragments including the Aβ peptide did not change. The lack of an effect on Aβ-species was also confirmed in ELISA studies revealing an increase in Aβ in the one and three-month-old 5xFAD mice as compared to wild-type mice (Fig. 4E). However, rhproCTSD dosing did not change these levels in neither sample fraction. Additionally, we compared the amounts of $A\beta^{1-34}$, $A\beta^{1-38}$, $A\beta^{1-40}$, $A\beta^{1-42}$ of 3-months-old wild-type and 5xFAD mice via 4-plex MSD assays (Liebsch et al., 2019) (Supplementary Fig. S4 F) but failed to detect changes after treatment. It is of note that when cerobrospinal fluid (CSF) was investigated in one-month-old mice rhproCTSD treatment even increased the levels of $A\beta^{1-42}$ (Fig. 4 F). To analyze the stability of the applied recombinant CTSD in mice we compared samples from one, two and three months old wild-type and 5xFAD mice injected either with PBS or rhpro-CTSD by immunoblot and an CTSD activity assays (Supplementary Fig. S4 G-I). We found an increased CTSD activity and expression in the one month old 5xFAD mice treated with rhpro-CTSD. The expression of the mature form of CTSD was still increased in two months old mice. It is of note that there was no increased CTSD activity measurable at two and three-month-old mice. Taken together, we did not find evidence for an obvious effect of CTSD treatment on Aβ levels as well on soluble and intracellular APP fragments.

2.5. Plaque morphology, number and neuroinflammation after intracranial rhproCTSD dosing in the 5xFAD mouse model

Despite the fact that our biochemical analysis did not reveal alterations in the expression levels of Aβ peptides we studied plaque formation, number and morphology after intracerebrally dosing the rhproCTSD. Using staining for Aβ and LAMP-1, as an indicator for the presence of lysosomes we observed in both PBS- and rhproCTSD-treated three-month-old brain cortices the formation of plaques which were surrounded by LAMP-1-positive cells (Fig. 5A). Calculation of the number of these structures in cortices and hippocampus did not reveal differences when PBS-injected and rhproCTSD-dosed mice were compared (Fig. 5B, Supplementary Fig. S5 A). Since the used E610 antibody also detects soluble Aβ fragments we also applied AmyloGlo staining (Schmued et al., 2012) to selectively stain amyloid plaques (Fig. 5C). The number of plaques and the plaque size in cortices and hippocampus was not affected after rhproCTSD dosing in the 5xFAD model (Fig. 5D, Supplementary S5 B). To not exclude earlier signs associated with the neurodegenerative process in the 5xFAD model we were interested if the treatment would affect neuroinflammation exerted by microglia and astroglia cells. Both, the degree of microgliosis (Fig. 5 E, F) and astrogliosis (Fig. 5 G, H; Supplementary Fig. S5 D) as judged by immunostaining and a ramification analysis (Fig. 5F, Supplementary Fig. S5 C) with Iba1 and GFAP did not change in the brains of three-month-old 5xFAD mice after having received rhproCTSD. These data clearly show that treatment with rhproCTSD did not affect the development of neuroinflammation which corresponds with a lack of an effect of the therapeutic enzyme on the levels of Aβ species.

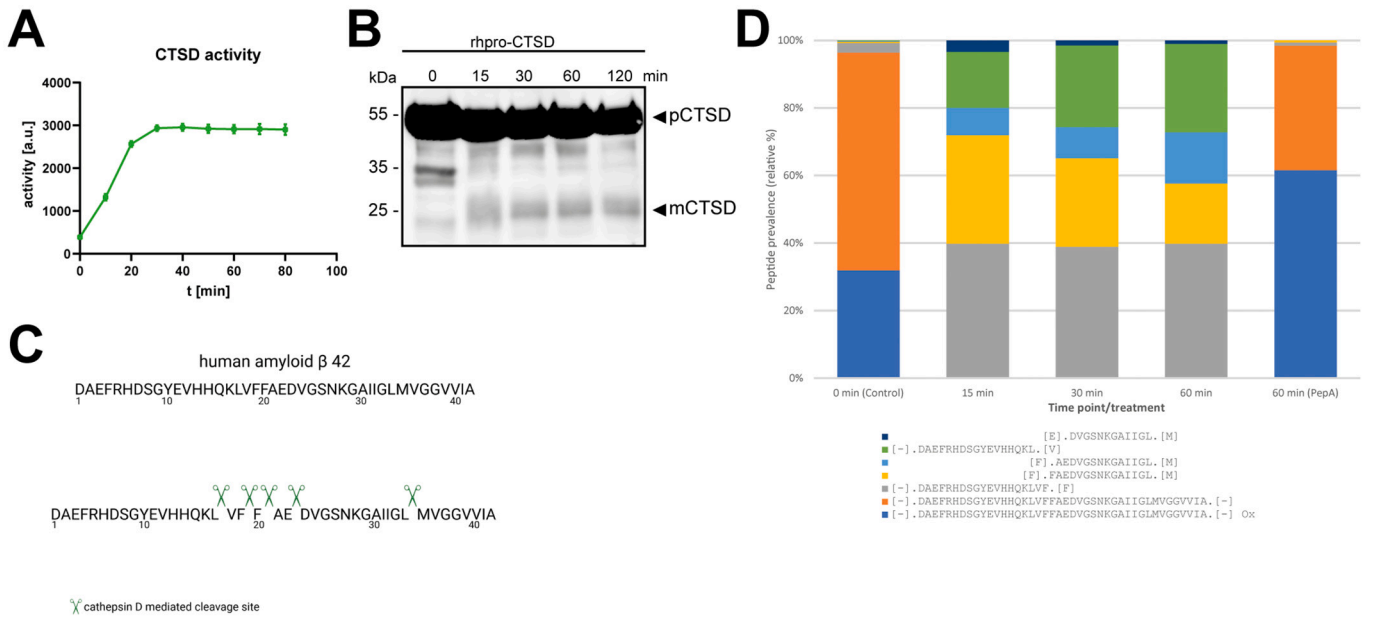

Fig. 1. *In vitro* digestion of Amyloid beta by recombinant human cathepsin-D. A The graph shows the measured CTSD-activity of self-activated rhproCTSD over time at pH 4.5. By cleaving a quenched CTSD-substrate the fluorescence intensity can be measured after excitation at 360 nm. B Western Blot of pre-incubated rh-pro-CTSD in processing buffer (0.1 M Tris-HCl, 3 mM EDTA, 5 mM Cysteine pH 4.5) shows activation of proCTSD (pCTSD) into mature CTSD (mCTSD). C Determined cleavage sites by rhCTSD within human aβ1–42. D Most abundant peptides identified following enzymatic digestion of aβ1–42 after 0 min (Control), 15 min, 30 min, or 60 min), or protease treatment plus the addition of pepstatin A (PepA, 60 min. incubation). Peptides detected with >9 peptide spectral matches (PSM) are shown, peptide prevalence was plotted as a percentage of the total PSM counts for each time point/treatment.

3. Discussion

The *endo*-lysosomal system has long been regarded as one of the most important intracellular factors affecting the molecular pathogenesis in AD. It has been realized that autophagic/lysosomal dysfunction and deficient lysosomal proteolysis contribute to the development of AD (Nixon, 2017). This assumption is supported by a boosted lysosomal proteolysis seen in an AD-mouse model after removal of cystatin B, an endogenous inhibitor of lysosomal cysteine proteases which led to an improvement of the Aβ levels, amyloid depositions and cognitive deficits (Yang et al., 2011). It is of note that different cystatins act in different ways, *i.e.* cystatin B is localized within the lumen of lysosomes (Yang et al., 2011) inhibiting cysteine proteases (*e.g.* cathepsin B,L,S,H), while cystatin C is found in the cytosol under oxidative stress conditions, protecting the cells from cathepsin leakage into cytosol (Watanabe et al., 2014).

Another study showed accelerated Aβ deposition after pepstatin A treatment, an aspartic protease inhibitor (Yamada et al., 1996). Furthermore, recent observation highlighted that dysfunctional autophagosomes are the basis of intracellular fibrillar Aβ accumulation (Lee et al., 2022).

CTSD has raised attention as a therapeutic target in AD (Di Domenico et al., 2016) through a considerable number of studies. The importance of CTSD as a principle lysosomal protease for lysosomal proteolysis in neurons is illustrated by the severe neurodegeneration associated with a lack of the protease in human, mice and sheep (Saftig et al., 1995; Steinfeld et al., 2006; Tyynela et al., 2000). The lack of CTSD leads to the congenital variant NCL10 of neuronal ceroid lipofuscinosis, severe lysosomal storage diseases (LSD) with accumulation of protein aggregates, blindness and neuronal death (Jalanko and Braulke, 2009). Prompted by the successful application of a "protease replacement therapy" in the NCL10 model leading to an improvement of neuropathology and lifespan extension (Marques et al., 2020) and clinically approved approaches to treat LSDs even with severe neurological manifestations (Schulz et al., 2018) we studied the efficacy of such a novel potentially therapeutic approach in cellular and animal models of AD. This was encouraged also by exogenously applied rhproCTSD that led to a decrease of pathological α-synuclein conformers *in vivo* and a restoration of *endo*-lysosome and autophagy function (Prieto Huarcaya et al., 2022). In AD, the pathological hallmarks are accumulations of Aβ and tau proteins and reduced clearance of both through the autophagy-lysosomal system has been suggested (Nixon and Yang, 2011). Therefore, we have chosen an approach to foster lysosomal proteolysis by supplying additional cathepsin-D in cell-based and *in vivo* models of AD with an increased expression of APP and accumulation of Aβ. This was especially relevant since studies implicated CTSD in the processing of APP forms (Ladror et al., 1994), in degradation of tau (Kenessey et al., 1997) and Aβ (Suire et al., 2020), respectively. *In vitro* the principle ability of the pre-activated CTSD to cleave in a time-dependent fashion $A\beta^{1-42}$ could be confirmed. CTSD endopeptidase cleavage prefers hydrophobic residues at P1 (Sun et al., 2013) and such residues are present within the Aβ sequence at positions Phe4, Leu17, Phe19, Phe20, and Leu34. Our LC-MS analysis of the *in vitro* digestion verifies these positions except from Phe4. Additionally, a CTSD-mediated cleavage site is shown for Glu22. In the NCL10 model pathological accumulation of proteins and a defect in autophagic flux could be reversed (Marques et al., 2020; Liu et al., 2022) after intracerebral and intravitreal dosing of rhproCTSD. However, the successful delivery of CTSD to lysosomes in different cell types of the CNS did not apparently affect APP processing, stability of APP CTFs and the level of Aβ. This is also in accordance with early studies that failed to show a direct role of CTSD in neuronal APP processing (Saftig et al., 1996). *In cellula* experiments studying cells with an overexpression of wildtype and the Swedish mutant of APP revealed that also in this set up, despite successful uptake and maturation of exogenously added CTSD, no significant impact of the protease in APP processing and the generation of soluble APP fragments including Aβ could be observed. Most importantly, we also intracerebrally applied pro-CTSD very early to one of the best described AD mouse models, the 5xFAD mice. Careful analysis of the brains of these mice after one, two and three months of age did not reveal a therapeutic effect in terms of a reduction of Aβ species, reduced plaque burden and neuroinflammation. Despite that, we focused on the early stages of pathology in these mice it

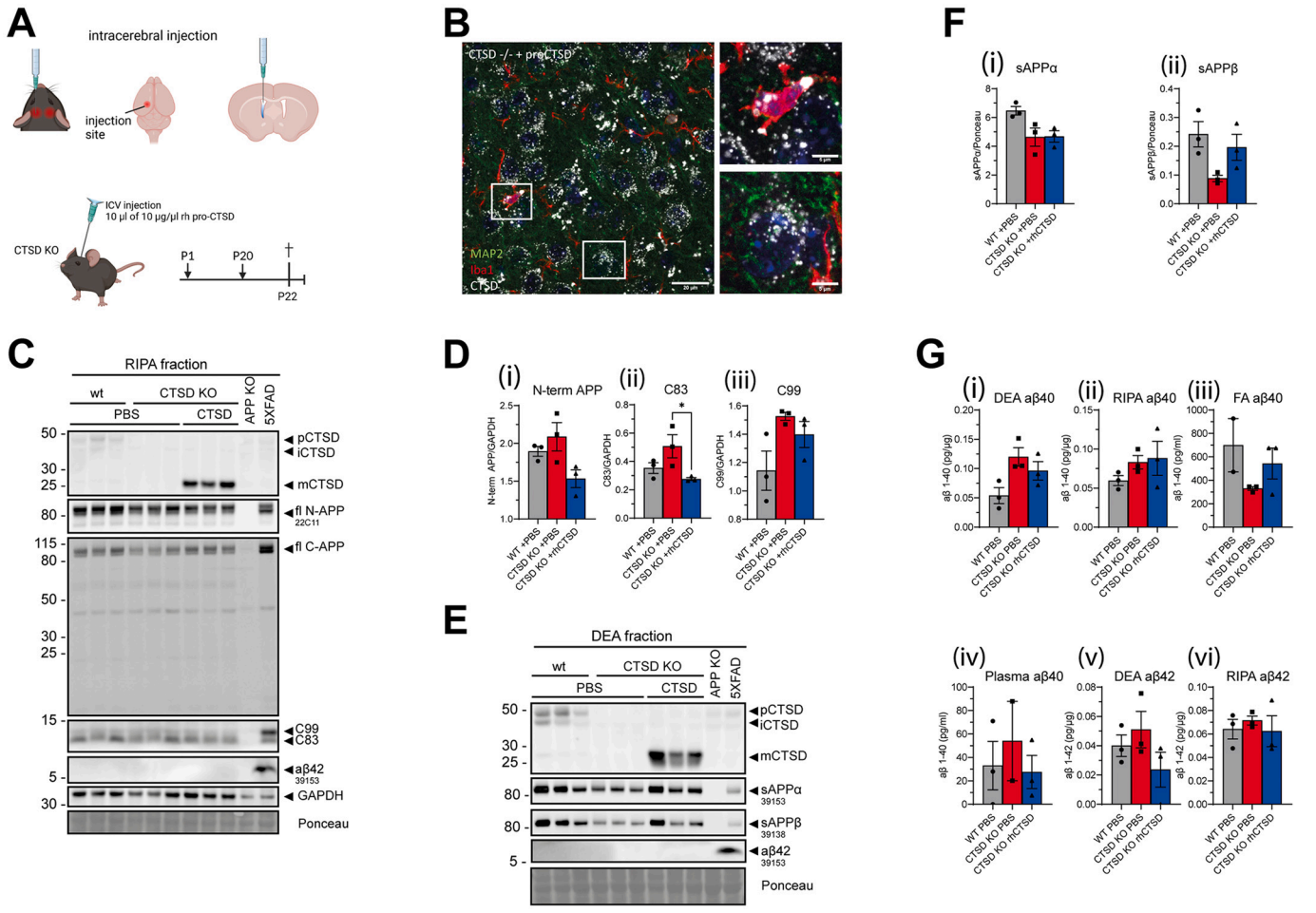

Fig. 2. Intracranial injection with rhproCTSD of CTSD-deficient mice has no evident effect on APP processing. A Scheme of intracranial injection area and time schedule for CTSD KO mice. B Immunohistochemistry of the cortex of P23 CTSD-deficient mice injected with 0,1 mg rhproCTSD shows the neuronal marker MAP2, the microglia marker Iba1 and CTSD. Nuclei are stained with DAPI Scale bar: 20 µm, insert: 5 µm. C Immunoblot of RIPA samples from brains of P23 WT mice treated with PBS and CTSD-deficient mice injected with either PBS or 0,1 mg rhproCSTD. Antibodies directed against epitopes of cathepsin-D, APP and aβ1–42 were used. Brains from APP KO and 5xFAD served as an antibody control ($n = 3$). D Quantifications of full-length APP and C-terminal fragments C83 and C99. GAPDH was used as loading control. E Immunoblot of DEA samples from brains of P23 WT mice injected with PBS and CTSD-deficient mice injected with either PBS or rhproCTSD along with control samples from brains of APP KO and 5xFAD mice. Antibodies directed against epitopes of cathepsin-D, APP and $a\beta^{1-42}$ were used. F Quantification of soluble APP fragments, normalized to Ponceau S staining (n = 3). G ELISA analysis of RIPA, DEA, FA brain samples and plasma from P23 WT mice injected with PBS and CTSD-deficient mice with PBS or 0,1 mg rhproCTSD (n = 3). Data represent mean ± SEM. Statistical analysis was performed by using one-way ANOVA with a Tukey's multiple comparison test. ** $p < 0.01$, * $p < 0.05$.

is conceivable that the dramatic and continuous production of Aβ in these AD mouse model (Manji et al., 2019) would have masked a possible therapeutic effect of CTSD. However, our analyses of the NCL10 mouse model as well as in the HEK cell system where also no effect of CTSD was observed argue against this assumption. Of note, CTSD application raised the level of $A\beta^{1-42}$ in the CSF of 5xFAD mice. It was suggested that CTSD may have a BACE1-like activity on APP especially when the Swedish version of APP is expressed (Hook et al., 2008) This could indicate that an increase of CTSD activity leads to a preference towards full length APP compared to Aβ. It is also conceivable that CTSD increases CSF $A\beta^{1-42}$ levels in an indirect way by accelerating the maturation of other lysosomal enzymes such as the cysteine protease CTSB. Similar to CTSD and BACE1, also CTSB as a cysteine hydrolase may act as with a BACE1-like activity (Hook et al., 2005).

3.1. Limitation of the study and perspectives

Our selected approach with the 5xFAD model was to accelerate lysosomal proteolysis by dosing rhproCTSD as early as possible to lower Aβ levels as soon as they might appear. However, despite a relative long half-life of the dosed enzyme (Marques et al., 2020) in mouse brain we were unable to detect significant activity of the enzyme at two and three months of age. A regular dosing protocol for longer periods may be suited to judge "therapeutic" effects at later stages. It should, however be noted that the progressive nature of the Aβ pathology observed in the 5xFAD mice may counteract any expected positive effect of the treatment at later time points.

Despite that, we have disproven our initial hypothesis that an exogenous delivery of the principle lysosomal protease CTSD assists in the amyloid degrading pathway, the lack of a therapeutic effect also raises important questions for future research. How important are lysosomal proteases for APP and Aβ metabolism? Does one require an application of a mixture of lysosomal proteases both active as *endo-* or exopeptidase to allow sufficient breakdown and disappearance of Aβ species? Our recent study where an application of cathepsin B and L for the removal of protein aggregates in neurodegeneration was investigated (Di Spiezio et al., 2021) suggested a hierarchical process of activities of both cysteine and aspartyl proteinases. In summary, lysosomal protease supplementation may be a useful approach to remove unwanted protein accumulation by improving lysosomal proteolytic

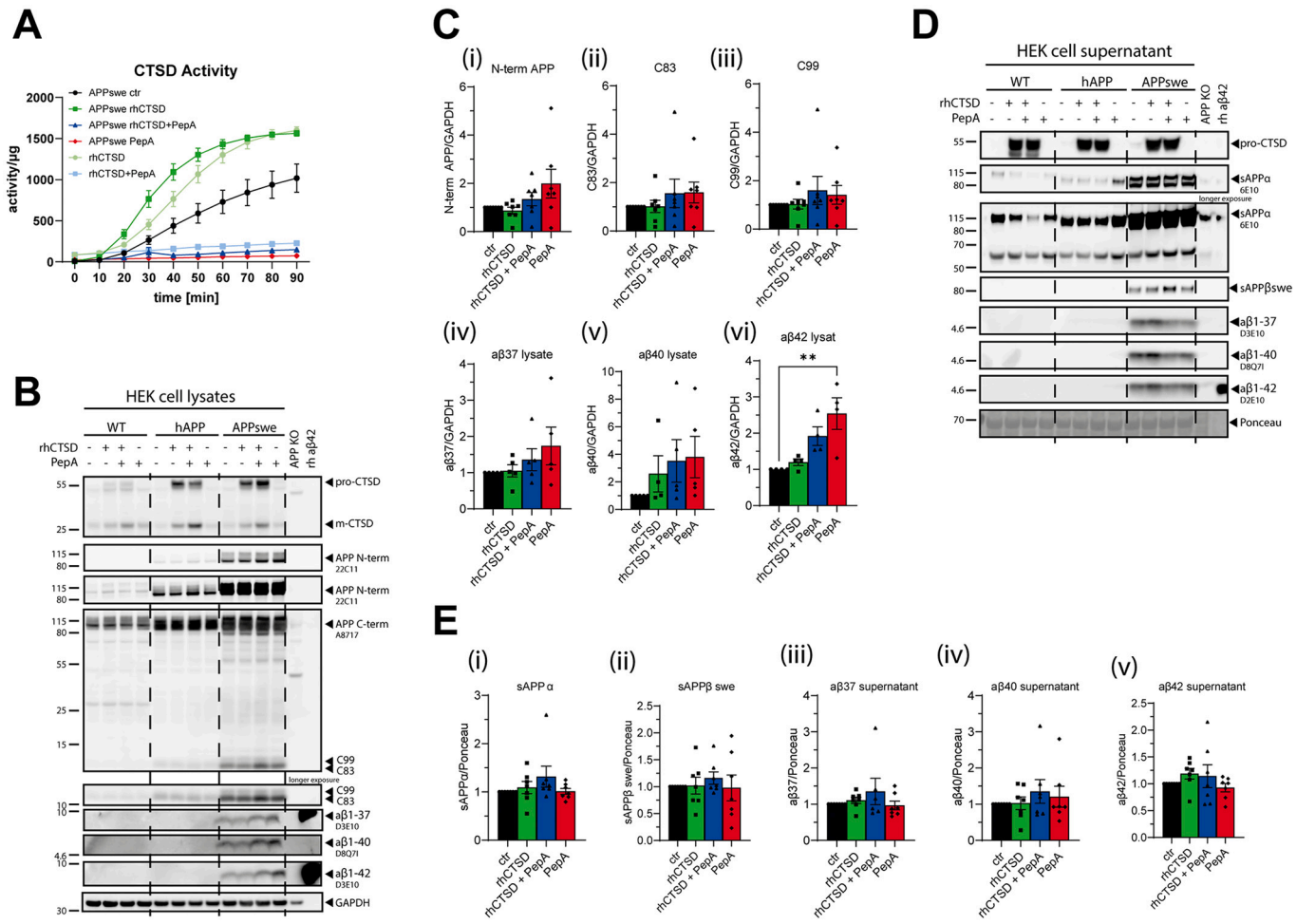

Fig. 3. Inhibition of Cathepsin-D increases cellular amyloid β 42 in HEK APPswe cells. A Cathepsin-D activity assayed with an artificial fluorescent substrate in HEK WT, hAPP and APPswe cell lysates over a time period of 90 min. B Immunoblot of cell lysates of HEK WT, hAPP and APPswe cells treated with 20 µg/ml rhproCTSD with or without 10 µg/ml pepstatin A (PepA). APP KO mouse brain lysates and human aβ1–42 protein served as antibody controls. Antibodies directed against cathepsin-D, various epitopes of APP and aβ species were used. C Quantifications of N- and C-terminal APP and amyloid β fragments of cell lysates from (B). GAPDH served as loading control ($n = 4$–7). D Immunoblot of supernatant of cells shown in (B). Antibodies detecting, CTSD, soluble APPα and APPβ and various aβ species were used. Ponceau S staining was used to verify equal loading amounts. E Quantifications of samples from (D) ($n = 6$–7). Ponceau S staining served as loading control. Data represent mean ± SEM. Statistical analysis was performed by using one-way ANOVA with a Tukey's multiple comparison test. ** $p < 0.01$, * $p < 0.05$.

degradation. However, in the case of Aβ degradation most likely more than one lysosomal protease has to act in concert.

4. Material and methods

4.1. Cell lines and treatment

Human Embryonic Kidney (HEK) WT and overexpressing human Amyloid Precursor Protein (HEK hAPP) and Swedish mutated APP (HEK APPswe) cells were cultured in Dulbecco's modified Eagle Medium (DMEM) containing 4.5 g/L of D-Glucose and L-glutamine (Thermo Fisher Scientific) and were supplemented with 10% (*v*/v) fetal bovine serum (FBS) and 1% Penicillin/Streptomycin (Pen/Strep). HEK hAPP and HEK APPswe cells were additionally treated with 200 µg/ml Geneticin (G418, Invivogen). Cells were cultivated at 37 °C/ 5% CO2. Cells were plated into 6 cm-dishes one day before any assay was implemented. For the treatment with recombinant proCTSD (rhproCTSD) cells were carefully washed three times with PBS and 20 µg/ml and/or 10 µg/ml Pepstatin A (PepA) was added to DMEM containing 1% FBS and 1% Pen/Strep for 48 h.

4.2. Mouse models and intracranial injection

In agreement with the German animal welfare law all animal handling and care were performed according to the guidelines of the Christian- Albrechts-University of Kiel. The Ministry of Energy, Agriculture, the Environment and Rural Areas Schleswig-Holstein approved animal experiments under the reference number V242–40536/2016 (81–6/16). All mice were housed in individually ventilated cage (IVC) under a 12 h light/12 h dark cycle with free access to food (pellets by Sniff Spezialdiäten, V1534) and water. Mice cages were maintained in a room with a temperature between 19 and 22 °C and humidity of 45–60%.

CTSD-deficient mice (NCL10 model) were obtained from heterozygotes matings and genotyped as previously described (Saftig et al. 1995). 5xFAD mice (AD model, expressing human APP and PSEN1 transgenes with a total of five AD-linked mutations: Swedish (K670N/M671L), Florida (I716V), and London (V717I) mutations in APP, and the M146L and L286V mutations in PSEN1) were generated with a C57BL/6 N background and genotyped for its transgenic mutations in PSEN1.

Intracranial injections with 10 µl of 10 µg/µl recombinant procathepsin D (purified as described in (Marques et al., 2020)) were performed at P1 and P20 for both CTSD-deficient and 5xFAD mice as

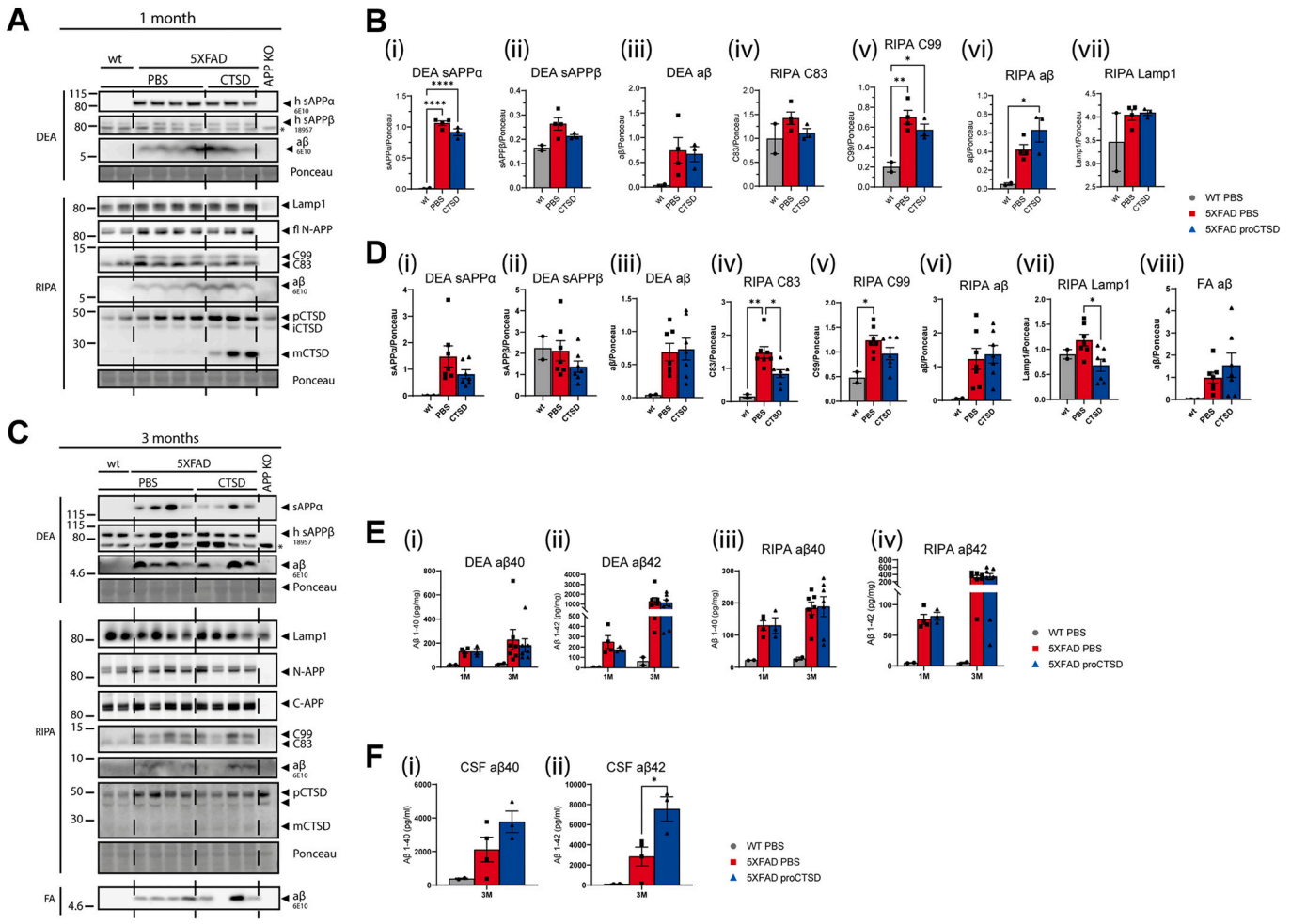

Fig. 4. Intracranial injection with rhproCTSD of 5xFAD mice has no beneficial effect on preventing aβ load within the mouse brain. A Immunoblot of soluble and membrane bound protein fractions from brain hemispheres of one-month-old female WT and 5xFAD mice intracranially injected with either PBS or 0,1 mg rhproCTSD at P1 and P20. Antibodies detecting CTSD, Lamp-1, various APP species and aβ were used. Brain lysate of an APP KO mice was used as antibody control for APP antibodies. Ponceau S staining served as loading control. B Quantitative analysis of one-month-old female 5xFAD shown in (A) ($n = 2$–4). C Representative immunoblot of DEA, RIPA an FA fractions from brain hemispheres of three-month-old female WT and 5xFAD mice intracranially injected with either PBS or 0,1 mg rhproCTSD at P1 and P20. Antibodies directed against epitopes of CTSD, Lamp1, various APP species and aβ were used. APP KO brain lysate was used as an antibody control for APP antibodies. Ponceau S staining verified equal loading amounts. D Quantitative analysis of three-month-old female 5xFAD shown in (C) (WT: $n = 7$, 5xFAD: n = 7). E ELISA analysis of samples used in (A) and (C). (one month: WT: n = 2, 5xFAD: n = 3–4; three months: WT: n = 2, 5xFAD: n = 7). F ELISA analysis of CSF (cerebrospinal fluid) collected from one-month-old 5xFAD injected with either PBS or 100 µg rhproCTSD (n = 2–4). Data represent mean ± SEM. Statistical analysis was performed by using one-way ANOVA with a Tukey's multiple comparison test. **** $p < 0{,}001$, *** $p < 0{,}005$, ** $p < 0.01$, * $p < 0.05$.

previously described (Marques et al., 2020). Briefly, mice were anaesthetized using isoflurane (2% in oxygenized air). The PBS or proCTSD was injected in the cauda putamen with a microsyringe (30 G) using a spacing devise with an injection depth of 1.15 mm over a period of 3 min. Injections in pups P1 were done in the right hemisphere, while P20 injections were done in the left hemisphere. For transcardially perfusion with 0.1 M phosphate buffer CTSD-deficient mice were anaesthetized by intraperitoneal injection of 10 mg/ml Ketamine (Bremer Pharma GmbH, 26,706) and 6 mg/ml Rompun® (Bayer, KPOCCNU) in 0.9% (*w/v*) NaCl solution and at P22 (Fig. 2A) and 5xFAD after one, two or three months (Supplement Fig. S4 B). Brains were collected, the right hemisphere fixed with 4% PFA (paraformaldehyde) for immunohistochemistry and the left hemisphere was snap-frozen in liquid nitrogen for biochemical analysis.

4.3. Western blot analysis

Cells were washed three times in ice cold PBS and lysed in RIPA buffer (50 mM Tris-Cl, 150 mM NaCl, 1% NP-40, 0.05% sodium deoxycholate, 0.01% SDS, pH 7.5), supplemented with 1× (Roche, 11836145001) on ice for 1 h. Lysates were cleared by centrifugation at 13.000 rpm for 10 min at 4 °C. Brain lysates were generated by DEA extraction for soluble proteins followed by RIPA extraction for membrane and cytosolic proteins and FA extraction for insoluble proteins. Tissue was first homogenized with porcelain beads (PeqLab) in DEA buffer (50 mM NaCl, 0,2% diethylamine, pH 10) with 1× complete Protease Inhibitor Cocktail with a Precellys® 24 homogenizer (Bertin) at 6500 g for 30 s at 4 °C. The supernatant was cleared by ultracentrifugation at 130.000 *g* for 1 h at 4 °C. The supernatant contains soluble proteins while the resulting pellet was further resuspended in RIPA buffer (20 Mm Tris-HCl [pH 7,5], 150 mM NaCl, 1 mM Na_2EDTA, 1% NP-40, 1% sodium deoxycholate, 2,5 mM sodium pyrophosphate) and dissolved with Precellys at 6500 g for 30 s at 4 °C. After centrifugation at 5000 *g* for 10 min at 4 °C the supernatant was ultracentrifuged again at 130.000 rpm for 1 h at 4 °C. The supernatant contains the membrane bound proteins. The first pellet from the RIPA lysate contains insoluble proteins which gets resuspended in 70% formic acid (FA fraction) and again ultracentrifuged at 130.000 rpm for 1 h at 4 °C. The resulting

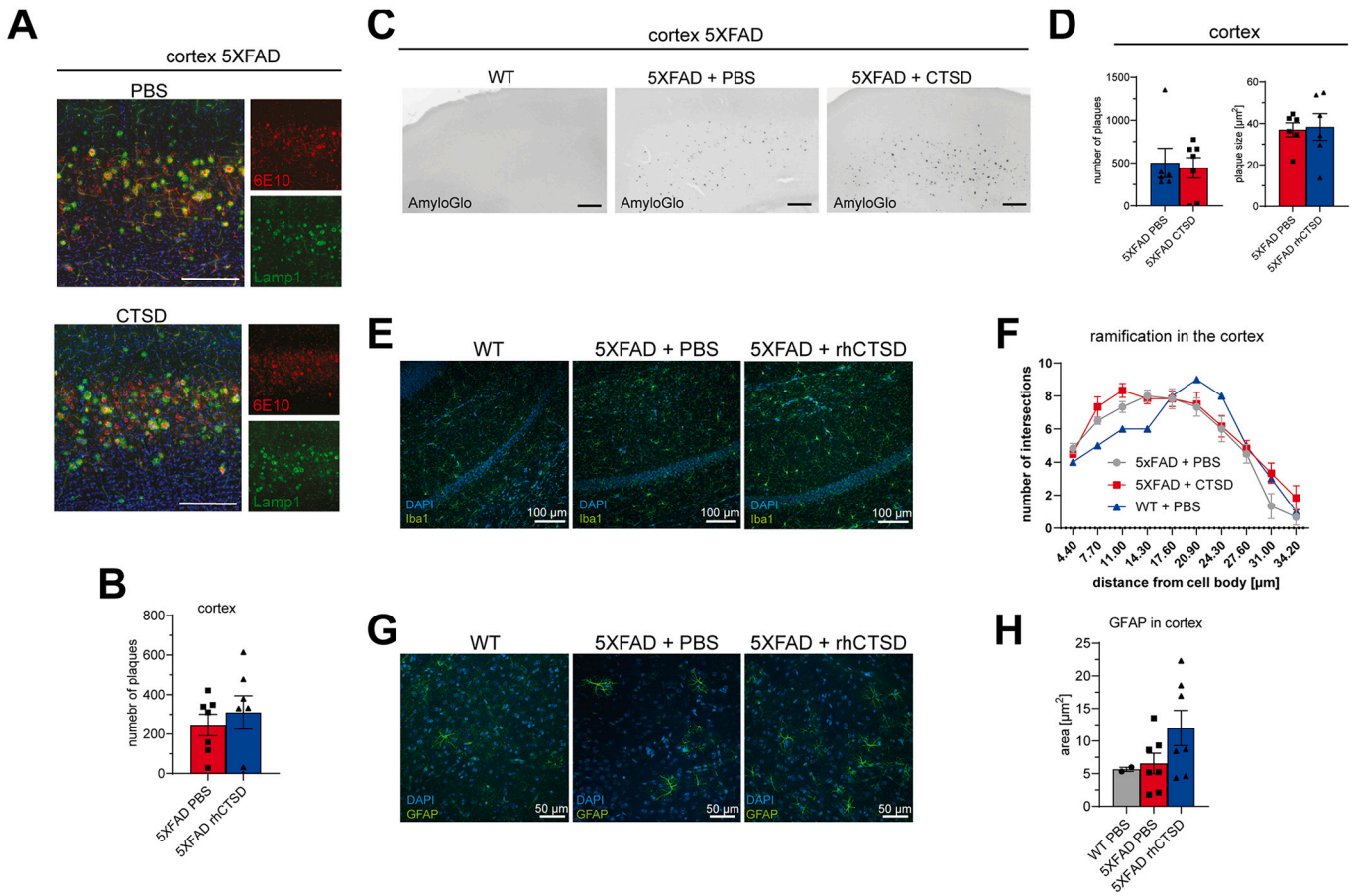

Fig. 5. Intracranial injection with rhproCTSD of 5xFAD mice does not lead to advantages on clearing aβ and does not prevent inflammation in 5xFAD brain. A Immunostainings from stained with DAPI (blue), anti-aβ (red, 6E10, Biolegend) and Lamp-1 (green, 1D4B, DSHB). Scale bar: 500 µm. B Counted aβ plaques in cortex of three-month-old female 5xFAD mice double injected with either PBS or 0,1 mg rhCTSD (n = 7). C Staining of aβ plaques with Amylo-Glo RTD Amyloid Plaque Stain Reagent (Biosensis) from cortex of three-month-old female 5xFAD mice double injected with either PBS or 0,1 mg rhproCTSD. Scale bar: 200 µm. D Number and size (μm^2) of aβ plaques from cortex (n = 7). E Immunostainings of microglia (Iba1, GeneTex, green) of the hippocampus of three-month-old female 5xFAD mice double injected with either PBS or 0,1 mg rhproCTSD. Nuclei are stained with DAPI (blue, Sigma-Aldrich). Scale bar: 100 µm. F Ramification analysis of microglia (Iba1-positive) in the cortex of three-month-old female 5xFAD mice double injected with either PBS or 0,1 mg rhproCTSD (n = 7). G Immunostainings of astrocytes (GFAP, Sigma-Aldrich, green) from the cortex of three-month-old female 5xFAD mice double injected with either PBS or 0,1 mg rhproCTSD. Nuclei are stained with DAPI (blue). Scale bar: 50 µm. H Analysis of the GFAP-positive area (μm^2) in the cortex of three-month-old female 5xFAD mice double injected with either PBS or 0,1 mg rhproCTSD (n = 7). Data represent mean ± SEM. (For interpretation of the references to colour in this figure legend, the reader is referred to the web version of this article.)

supernatant contains insoluble proteins. Protein concentration was determined using the BCA assay (Thermo Fisher Scientific) and denatured with 5× Laemmli (60 mM Tris-Cl pH 6.8, 2% SDS, 10% glycerol, 5% β-mercaptoethanol, 0.01% bromophenol blue) for 5 min at 95 °C. Equal amounts of denatured lysates were separated by electrophoresis on 4–12% NuPage gradient gels (Thermo Fisher Scientific, NP0336BOX) continuously running at 80 V. Then, proteins were transferred to a nitrocellulose membrane (Whatman, GE Healthcare, 10426994) using wet blotting. The membranes were blocked for 30 min with 5% dry milk in TBS-T (20 mM Tris/HCl pH 7.0, 150 mM NaCl, 0.1% (*v*/v) Tween® 20). The following primary antibodies were used: 1:1000 rat anti-Lamp1 (1D4B, Developmental Studies Hybridoma Bank, Iowa City, IA, USA), 1:1000 mouse anti-Lamp1 (H4A3, DSHB), 1:500 goat anti-CTSD (AF1014, R&D Systems), 1:2000 mouse anti-tubulin (E7, DSHB), 1:2000 rabbit anti-GAPDH (sc-25778, Santa Cruz Biotechnology), 1:1000 rabbit anti-APP (A8717, Sigma), 1:1000 mouse anti-APP (22C11, Thermo Fisher Scientific), 1:1000 mouse anti-β-Amyloid (6E10, Biolegend), 1:1000 rabbit anti-β-Amyloid (18058, Biolegend), 1:1000 rabbit anti-sAPPβ-WT (18957, IBL), 1:2000 mouse anti-sAPPβ-swe (6A1, IBL), β-Amyloid Antibody Sampler Kit (85314T, Cell Signaling). Afterwards, blots were washed with TBS-T for 30 min and incubated for 1 h at RT with 1:10.000 secondary antibodies coupled to horseradish-peroxidase (HRP) (goat anti-rabbit HRP, rabbit anti-goat HRP, goat anti-mouse HRP, goat anti-rat HRP) in blocking solution. Horseradish peroxidase activity was detected by ImageQuant™ LAS 680 (GE Healthcare) after incubation with Amersham ECL Advanced Western Blotting Detection kit (GE Healthcare, RPN2135).

4.4. Immunostainings

Mouse brains were fixed in 4% PFA for 4 h to be subsequently washed in phosphate buffer (PB) at 4 °C overnight, immersed in 30% sucrose in PB, and stored at 4 °C. Sections (35 µm) were cut sagittal with a Leica SM 2000R sliding microtome (Leica Microsystems) with dry-ice cooling and stored in PB containing 0.02% (*w*/*v*) sodium azide. Floating slides were washed three times with PB, blocked and permeabilized 0.5% Triton X-100, 4% normal goat serum (Gibco) and incubated overnight with rabbit 1:750 anti-Iba1 (GTX100042, GeneTex), mouse anti-GFAP (G3893, Sigma), 1:500 rabbit anti-CTSD (kindly provided by Prof. Andrej Hasilik, Münster), 1:750 rat anti-Lamp1 (1D4B, DSHB) and 1:300 mouse anti-β-Amyloid (6E10, Biolegend) antibodies in blocking solution. After three washing steps with 0.25% Triton X-100 in PB,

sections were incubated with 1:750 Alexa Fluor-conjugated secondary antibodies (A21208 donkey anti-rat 488, A21202 donkey anti-mouse 488, A21203 donkey anti-rabbit 594, A21203 donkey anti-mouse 594, A78947 donkey anti-rat 647, A31573 donkey anti-rabbit 647, A21447 donkey anti-goat 647, Thermo Fisher Scientific) for 3 h at room temperature, washed again 3 times in washing buffer, and finally coverslipped in Mowiol/DABCO. For AmyloGlo staining the brain sections were dried at 55 °C on a gelatin-coated slide, transferred into a 70% ethanol solution for 5 min, washed in water and then incubated for 10 min with the AmyloGlo staining solution. Slides were briefly rinsed with 0,9% saline solution and coverslipped in Mowiol/DABCO. Imaging was performed on the Zeiss laser scanning microscope 980 with Airyscan 2 (Zeiss) or the Keyence fluorescence microscope BZ-X 800 (Keyence).

4.5. ELISA

To quantify mouse and human amyloid β 1–40 and 1–42 from CTSD-deficient and 5xFAD mice the DEA, RIPA and FA factions were analyzed after total protein determination by using the ELISA Kits from IBL (27718, 27719, 27720, 27721, IBL). To also determine amyloid β in the CSF, the mice were anaesthetized and the CSF was collected from the cisterna magna compartment using a glass capillary. The CSF was snap-frozen in liquid nitrogen until usage for ELISA. The assay was performed according to the supplier's manual.

4.6. MSD assay

An electrochemiluminescence-based assay was developed (neo-epitope specific Aβ34 and the sulfo-tagged 6E10 (binds to the N-terminus of human Aβ) or the sulfo-tagged 4G8 for rodent samples (binds to the mid domain of Aβ)) using the ELISA Conversion Kit from MSD (USA). High-bind or custom-printed 4-plex plates (using our mab34, 4G8 (Biolegend) for pan-Aβ assay, G2–10 for 1-plex Aβ40 assay, and MSD's validated mouse monoclonal anti-Aβ38, anti-Aβ40, as well as anti-Aβ42 antibodies, see MSD Aβ peptide V-PLEX) were blocked (MSD 5% Blocker A in PBS) for 1 h at 22 °C and washed three times with PBS-Tween (PBS-T) for 1 min at 22 °C, loaded with SULFO-TAG TM 6E10 or 4G8 detection antibody (diluted to 1× in MSD Diluent 100) and sample or peptide calibrator (in MSD Diluent 35 or cell culture medium), and incubated for 16 h at 4 °C with shaking at 600 rpm. After three washing steps with PBS-T for 1 min at 22 °C, 150 µl 2× MSD read buffer was added per well. All plates were read using an MSD QuickPlex SQ 120 Imager and data analyzed using MSD Workbench® software. Standard curves were fitted using a non-linear four-parameter logistic fit.

4.7. Purification of recombinant human pro-cathepsin D

HEK 293-EBNA cells stable expressing pCEP-Pu containing pro-CTSD were grown in purification medium (DMEM, 2.5% FBS and 1% Pen/Strep for one week. Cell culture supernatant was collected, filtrated and concentrated *via* an Amicon system and an ultrafiltration disk with a 10 kDa cutoff (Millipore, PLGC07610). Recombinant protein was purified *via* its N-terminal His-Tag using a His-Trap 1 ml column (GE Healthcare, 29–0510-21) on an Aekta Purifier System (GE Healthcare) and eluted with 250 mM imidazole (Roth, X998.4) in PBS, pH 7.4. The protein was further purified via size exclusion chromatography on a Superdex 75 column (GE Healthcare, GE17–5174–1). Monomeric rhCTSD was concentrated using a Vivaspin 20 tube with 10 kDa cutoff (Sartorious, VS2002). The purified protein was stored at -20 °C.

4.8. Cathepsin activity assay

To measure Cathepsin D activity in cells, lysates were prepared in RIPA buffer without protease inhibitors to keep protease activity. Activity buffer (50 mM sodium acetate (pH 5.5), 0.1 M NaCl, 1 mM EDTA, and 0.2% Triton X-100) containing 10 µM of CTSD substrate (P-145, Enzo Life Sciences) together with tested sample and pre-activated rhproCTSD as control was incubated at 37 °C and the fluorescence was measured over a time of 90 min using a Synergy™ HT Multi-Detection microplate reader (exc: 360 nm; em: 440 nm, band pass 40).

4.9. Liquid chromatography-mass spectrometry (LC-MS)

To analyze the ability of our purified cathepsin D to cleave human recombinant amyloid β 42, pro-cathepsin D was pre-activated in 50 mM sodium acetate and 50 mM NaCl at pH 4.5 for 2 h at 37 °C and afterwards incubated with 100 µM of human amyloid β 42 (151–002, Enzo) with or without Pepstatin A at 37 °C. Samples were collected after 0, 15, 30 and 60 min and directly frozen at -20 °C and analyzed *via* LC-MS. Aliquots of the samples were diluted 1:100 in LC loading buffer (3% acetonitrile (ACN) and 0.1% trifluoroacetic acid in water), and transferred to glass autosampler vials. LC-MS analysis was performed on a Dionex U3000 nanoRSLC UHPLC (Thermofisher, Dreieich, Germany) equipped with an Acclaim PepMap100 column (2 µm particle size, 75 µm × 500 mm) and µ-precolumn (300 µm × 5 mm) coupled online to a Q Exactive HF mass spectrometer (Thermofisher, Bremen, Germany). The eluents used were; eluent A: 0.05% formic acid (FA), eluent B: 80% ACN + 0.05% FA. The separation was performed over a programmed 40-min run. Chromatographic conditions were: 4% B for 3 min followed by a linear gradient from 4% to 50% B over 10 min, a 2-min increase to 90% B, and 10 min at 90% B. Following this, an inter-run equilibration of the column was achieved by 15 min at 4% B. A constant flow rate of 300 nl/min was used and 1 µl of sample was injected per run. Acquisition of data was performed on the Orbitrap Q Exactive HF mass spectrometer utilizing HCD fragmentation at a normalized collision energy of 27. A full scan MS acquisition was performed (resolution 60,000) with subsequent data dependent MS/MS (resolution 15,000) of the top 10 most intense ions; dynamic exclusion was enabled (2 s duration).

Database searches were performed in Proteome Discoverer (Ver. 2.2.0.388) using the SequestHT search algorithm and combined database that included the Aβ1–42 peptide, cathepsin D, and the cRAP list of commonly occurring laboratory contaminants. Small database search criteria were employed in which a fixed PSM was used and only peptides assigned as high confidence (Maximum delta Cn:0.5).

4.10. Statistical analysis and data analysis

Data are shown as mean ± S.E.M. For statistical analysis one-way ANOVA was employed using GraphPad Prism 5 (Graph Pad Software, Inc., San Diego, USA): * $P < 0.05$; ** $P < 0.01$; *** $P < 0.001$; **** $P < 0.0001$.

The ramification analysis was done using the Sholl Analysis plugin in ImageJ (Fiji) with following setting: start radius: 4.4 µm, step size: 3.3 µm, end radius: 34,9 µm. For each brain sample two slides were analyzed in the hippocampal region (CA1, CA3 and dentate gyrus) and cortex.

Supplementary data to this article can be found online at https://doi.org/10.1016/j.nbd.2022.105919.

Funding

This work was supported in part by the Deutsche Forschungsgemeinschaft (SFB877, A3 and Z2) and the Canadian Institutes of Health Research – CIHR (to GM).

CRediT authorship contribution statement

Lisa Gallwitz: Conceptualization, Methodology, Investigation, Validation, Visualization. **Lina Schmidt:** Methodology, Investigation. **André R.A. Marques:** Methodology, Investigation. **Andreas Tholey:** Investigation, Formal analysis. **Liam Cassidy:** Investigation, Validation. **Irem Ulku:** Investigation, Validation. **Gerhard Multhaup:** Conceptualization, Supervision, Writing – original draft, Writing – review &

editing. **Alessandro Di Spiezio:** Conceptualization, Supervision, Writing – original draft, Writing – review & editing. **Paul Saftig:** Conceptualization, Supervision, Writing – original draft, Writing – review & editing.

Data availability

Data will be made available on request.

Acknowledgments

We would like to thank Marlies Rusch for her crucial technical support and François Cossais for the support with the Keyence microscope. We are also thankful for Ulrike Müller, Heidelberg University for providing APP-deficient murine brains for control experiments. Illustrations were created with BioRender.com

References

Chai, Y.L., Chong, J.R., Weng, J., Howlett, D., Halsey, A., Lee, J.H., et al., 2019. Lysosomal cathepsin D is upregulated in Alzheimer's disease neocortex and may be a marker for neurofibrillary degeneration. Brain Pathol. 29 (1), 63–74.

Davidson, Y., Gibbons, L., Pritchard, A., Hardicre, J., Wren, J., Tian, J., et al., 2006. Genetic associations between cathepsin D exon 2 C–>T polymorphism and Alzheimer's disease, and pathological correlations with genotype. J. Neurol. Neurosurg. Psychiatry 77 (4), 515–517.

Dean, R.T., 1975. Direct evidence of importance of lysosomes in degradation of intracellular proteins. Nature 257 (5525), 414–416.

Dean, R.T., Barrett, A.J., 1976. Lysosomes. Essays Biochem. 12, 1–40.

Di Domenico, F., Tramutola, A., Perluigi, M., 2016. Cathepsin D as a therapeutic target in Alzheimer's disease. Expert Opin. Ther. Targets 20 (12), 1393–1395.

Di Spiezio, A., Marques, A.R.A., Schmidt, L., Thiessen, N., Gallwitz, L., Fogh, J., et al., 2021. Analysis of cathepsin B and cathepsin L treatment to clear toxic lysosomal protein aggregates in neuronal ceroid lipofuscinosis. Biochim. Biophys. Acta Mol. basis Dis. 1867 (10), 166205.

Felbor, U., Kessler, B., Mothes, W., Goebel, H.H., Ploegh, H.L., Bronson, R.T., et al., 2002. Neuronal loss and brain atrophy in mice lacking cathepsins B and L. Proc. Natl. Acad. Sci. U. S. A. 99 (12), 7883–7888.

Hamazaki, H., 1996. Cathepsin D is involved in the clearance of Alzheimer's beta-amyloid protein. FEBS Lett. 396 (2–3), 139–142.

Hook, V., Toneff, T., Bogyo, M., Greenbaum, D., Medzihradszky, K.F., Neveu, J., et al., 2005. Inhibition of cathepsin B reduces beta-amyloid production in regulated secretory vesicles of neuronal chromaffin cells: evidence for cathepsin B as a candidate beta-secretase of Alzheimer's disease. Biol. Chem. 386 (9), 931–940.

Hook, V., Schechter, I., Demuth, H.U., Hook, G., 2008. Alternative pathways for production of beta-amyloid peptides of Alzheimer's disease. Biol. Chem. 389 (8), 993–1006.

Jalanko, A., Braulke, T., 2009. Neuronal ceroid lipofuscinoses. Biochim. Biophys. Acta 1793 (4), 697–709.

Katunuma, N., 2010. Posttranslational processing and modification of cathepsins and cystatins. Journal of Signal Transduction 2010, 375345.

Kenessey, A., Nacharaju, P., Ko, L.W., Yen, S.H., 1997. Degradation of tau by lysosomal enzyme cathepsin D: implication for Alzheimer neurofibrillary degeneration. J. Neurochem. 69 (5), 2026–2038.

Koike, M., Nakanishi, H., Saftig, P., Ezaki, J., Isahara, K., Ohsawa, Y., et al., 2000. Cathepsin D deficiency induces lysosomal storage with ceroid lipofuscin in mouse CNS neurons. J. Neurosci. 20 (18), 6898–6906.

Ladror, U.S., Snyder, S.W., Wang, G.T., Holzman, T.F., Krafft, G.A., 1994. Cleavage at the amino and carboxyl termini of Alzheimer's amyloid-beta by cathepsin D. J. Biol. Chem. 269 (28), 18422–18428.

Lee, J.H., Yang, D.S., Goulbourne, C.N., Im, E., Stavrides, P., Pensalfini, A., et al., 2022. Faulty autolysosome acidification in Alzheimer's disease mouse models induces autophagic build-up of Abeta in neurons, yielding senile plaques. Nat. Neurosci. 25 (6), 688–701.

Liebsch, F., Kulic, L., Teunissen, C., Shobo, A., Ulku, I., Engelschalt, V., et al., 2019. Abeta34 is a BACE1-derived degradation intermediate associated with amyloid clearance and Alzheimer's disease progression. Nat. Commun. 10 (1), 2240.

Liu, J., Bassal, M., Schlichting, S., Braren, I., Di Spiezio, A., Saftig, P., et al., 2022. Intravitreal gene therapy restores the autophagy-lysosomal pathway and attenuates retinal degeneration in cathepsin D-deficient mice. Neurobiol. Dis. 164, 105628.

Manji, Z., Rojas, A., Wang, W., Dingledine, R., Varvel, N.H., Ganesh, T., 2019. 5xFAD mice display sex-dependent inflammatory gene induction during the prodromal stage of Alzheimer's disease. J. Alzheimers Dis. 70 (4), 1259–1274.

Marques, A.R.A., Di Spiezio, A., Thiessen, N., Schmidt, L., Grotzinger, J., Lullmann-Rauch, R., et al., 2020. Enzyme replacement therapy with recombinant pro-CTSD (cathepsin D) corrects defective proteolysis and autophagy in neuronal ceroid lipofuscinosis. Autophagy 16 (5), 811–825.

McDermott, J.R., Gibson, A.M., 1996. Degradation of Alzheimer's beta-amyloid protein by human cathepsin D. Neuroreport 7 (13), 2163–2166.

Mullan, M., Crawford, F., Axelman, K., Houlden, H., Lilius, L., Winblad, B., et al., 1992. A pathogenic mutation for probable Alzheimer's disease in the APP gene at the N-terminus of beta-amyloid. Nat. Genet. 1 (5), 345–347.

Nixon, R.A., 2017. Amyloid precursor protein and endosomal-lysosomal dysfunction in Alzheimer's disease: inseparable partners in a multifactorial disease. FASEB Journal 31 (7), 2729–2743.

Nixon, R.A., Yang, D.S., 2011. Autophagy failure in Alzheimer's disease—locating the primary defect. Neurobiol. Dis. 43 (1), 38–45.

Oakley, H., Cole, S.L., Logan, S., Maus, E., Shao, P., Craft, J., et al., 2006. Intraneuronal beta-amyloid aggregates, neurodegeneration, and neuron loss in transgenic mice with five familial Alzheimer's disease mutations: potential factors in amyloid plaque formation. J. Neurosci. 26 (40), 10129–10140.

Papassotiropoulos, A., Lewis, H.D., Bagli, M., Jessen, F., Ptok, U., Schulte, A., et al., 2002. Cerebrospinal fluid levels of beta-amyloid(42) in patients with Alzheimer's disease are related to the exon 2 polymorphism of the cathepsin D gene. Neuroreport 13 (10), 1291–1294.

Prieto Huarcaya, S., Drobny, A., Marques, A.R.A., Di Spiezio, A., Dobert, J.P., Balta, D., et al., 2022. Recombinant pro-CTSD (cathepsin D) enhances SNCA/alpha-Synuclein degradation in alpha-Synucleinopathy models. Autophagy 18 (5), 1127–1151.

Riemenschneider, M., Blennow, K., Wagenpfeil, S., Andreasen, N., Prince, J.A., Laws, S. M., et al., 2006. The cathepsin D rs17571 polymorphism: effects on CSF tau concentrations in Alzheimer disease. Hum. Mutat. 27 (6), 532–537.

Saftig, P., Klumperman, J., 2009. Lysosome biogenesis and lysosomal membrane proteins: trafficking meets function. Nat. Rev. Mol. Cell Biol. 10 (9), 623–635.

Saftig, P., Hetman, M., Schmahl, W., Weber, K., Heine, L., Mossmann, H., et al., 1995. Mice deficient for the lysosomal proteinase cathepsin D exhibit progressive atrophy of the intestinal mucosa and profound destruction of lymphoid cells. EMBO J. 14 (15), 3599–3608.

Saftig, P., Peters, C., von Figura, K., Craessaerts, K., Van Leuven, F., De Strooper, B., 1996. Amyloidogenic processing of human amyloid precursor protein in hippocampal neurons devoid of cathepsin D. J. Biol. Chem. 271 (44), 27241–27244.

Schmued, L., Raymick, J., Tolleson, W., Sarkar, S., Zhang, Y.H., Bell-Cohn, A., 2012. Introducing Amylo-Glo, a novel fluorescent amyloid specific histochemical tracer especially suited for multiple labeling and large scale quantification studies. J. Neurosci. Methods 209 (1), 120–126.

Schulz, A., Ajayi, T., Specchio, N., de Los, Reyes E., Gissen, P., Ballon, D., et al., 2018. Study of intraventricular Cerliponase alfa for CLN2 disease. N. Engl. J. Med. 378 (20), 1898–1907.

Steinfeld, R., Reinhardt, K., Schreiber, K., Hillebrand, M., Kraetzner, R., Bruck, W., et al., 2006. Cathepsin D deficiency is associated with a human neurodegenerative disorder. Am. J. Hum. Genet. 78 (6), 988–998.

Suire, C.N., Abdul-Hay, S.O., Sahara, T., Kang, D., Brizuela, M.K., Saftig, P., et al., 2020. Cathepsin D regulates cerebral Abeta42/40 ratios via differential degradation of Abeta42 and Abeta40. Alzheimers Res. Ther. 12 (1), 80.

Sun, H., Lou, X., Shan, Q., Zhang, J., Zhu, X., Zhang, J., et al., 2013. Proteolytic characteristics of cathepsin D related to the recognition and cleavage of its target proteins. PLoS One 8 (6), e65733.

Tyynela, J., Sohar, I., Sleat, D.E., Gin, R.M., Donnelly, R.J., Baumann, M., et al., 2000. A mutation in the ovine cathepsin D gene causes a congenital lysosomal storage disease with profound neurodegeneration. EMBO J. 19 (12), 2786–2792.

Watanabe, S., Hayakawa, T., Wakasugi, K., Yamanaka, K., 2014. Cystatin C protects neuronal cells against mutant copper-zinc superoxide dismutase-mediated toxicity. Cell Death Dis. 5, e1497.

Yamada, T., Liepnieks, J., Benson, M.D., Kluve-Beckerman, B., 1996. Accelerated amyloid deposition in mice treated with the aspartic protease inhibitor, pepstatin. J. Immunol. 157 (2), 901–907.

Yang, D.S., Stavrides, P., Mohan, P.S., Kaushik, S., Kumar, A., Ohno, M., et al., 2011. Reversal of autophagy dysfunction in the TgCRND8 mouse model of Alzheimer's disease ameliorates amyloid pathologies and memory deficits. Brain 134 (Pt 1), 258–277.